

# *Arm retraction dynamics of entangled star polymers: a forward-flux sampling method study*

Article

Accepted Version

Zhu, J., Likhtman, A. E. and Wang, Z. (2017) Arm retraction dynamics of entangled star polymers: a forward-flux sampling method study. *The Journal of Chemical Physics*, 147 (4). 044907. ISSN 0021-9606 doi: <https://doi.org/10.1063/1.4995422> Available at <https://centaur.reading.ac.uk/71476/>

It is advisable to refer to the publisher's version if you intend to cite from the work. See [Guidance on citing](#).

To link to this article DOI: <http://dx.doi.org/10.1063/1.4995422>

Publisher: American Institute of Physics

All outputs in CentAUR are protected by Intellectual Property Rights law, including copyright law. Copyright and IPR is retained by the creators or other copyright holders. Terms and conditions for use of this material are defined in the [End User Agreement](#).

[www.reading.ac.uk/centaur](http://www.reading.ac.uk/centaur)

**CentAUR**

Central Archive at the University of Reading

Reading's research outputs online

# 1 **Arm Retraction Dynamics of Entangled Star Polymers: A Forward-Flux Sampling**

## 2 **Method Study**

3 Jian Zhu, Alexei E. Likhtman and Zuowei Wang\*<sup>1</sup>

4 *Department of Mathematics and Statistics, University of Reading,*  
5 *Reading RG6 6AX, UK*

6 The study of dynamics and rheology of well-entangled branched polymers remains a  
7 challenge for computer simulations due to the exponentially growing terminal relax-  
8 ation times of these polymers with increasing molecular weights. We present an effi-  
9 cient simulation algorithm for studying the arm retraction dynamics of entangled star  
10 polymers by combining the coarse-grained slip-spring (SS) model with the forward-  
11 flux sampling (FFS) method. This algorithm is first applied to simulate symmetric  
12 star polymers in the absence of constraint release (CR). The reaction coordinate for  
13 the FFS method is determined by finding good agreement of the simulation results  
14 on the terminal relaxation times of mildly entangled stars with those obtained from  
15 direct shooting SS model simulations with the relative difference between them less  
16 than 5%. The FFS simulations are then carried out for strongly entangled stars with  
17 arm lengths up to 16 entanglements that are far beyond the accessibility of brute force  
18 simulations in the non-CR condition. Apart from the terminal relaxation times, the  
19 same method can also be applied to generate the relaxation spectra of all entangle-  
20 ments along the arms which are desired for the development of quantitative theories  
21 of entangled branched polymers. Furthermore, we propose a numerical route to con-  
22 struct the experimentally measurable relaxation correlation functions by effectively  
23 linking the data stored at each interface during the FFS runs. The obtained star arm  
24 end-to-end vector relaxation functions  $\Phi(t)$  and the stress relaxation function  $G(t)$   
25 are found to be in reasonably good agreement with standard SS simulation results  
26 in the terminal regime. Finally, we demonstrate that this simulation method can  
27 be conveniently extended to study arm-retraction problem in entangled star polymer  
28 melts with CR by modifying the definition of the reaction coordinate.

## I. INTRODUCTION

Development of quantitative theories for predicting the dynamic and rheological properties of entangled branched polymers is of both fundamental and practical importance. In the past decades, theoretical efforts have been primarily based on the concept of tube model originally proposed by de Gennes, Doi and Edwards.<sup>1-3</sup> Different from entangled linear polymers where reptation, contour length fluctuations (CLF) and constraint release (CR) are the main relaxation mechanisms, reptation in branched polymers is strongly suppressed due to the effectively localized branch points. In the simplest case of symmetric star polymers, the stress relaxation is conjectured to proceed via CLF or arm retraction by which the free end of an arm retracts inward along the primitive path to escape from the original tube segments and pokes out again to explore new tube. Since arm retraction is entropically unfavorable and so thermally activated, this process can be formulated as a first-passage (FP) problem or Kramers problem.<sup>4-6</sup>

A star arm retracting in a fixed network experiences a potential barrier theoretically described by a quadratic function  $U(s) = \nu k_B T Z s^2$  where  $k_B$  is the Boltzmann constant,  $Z = M/M_e$  is the number of entanglements per arm,  $M$  is the arm molecular weight,  $M_e$  is the entanglement molecular weight and  $\nu$  is treated as a constant.<sup>7</sup> The fractional coordinate  $s$  measures the retraction depth of the arm free end. Pearson and Helfand predicted an exponential dependence of the arm terminal relaxation time,  $\tau_d$ , and correspondingly the viscosity,  $\eta_0$ , on the arm molecular weight,  $\eta_0 \sim \tau_d \sim \exp(\nu M/M_e)$ .<sup>8</sup> This prediction, however, shows a large discrepancy from experimental data obtained in star polymer melts due to the neglect of CR effects. Ball and McLeish<sup>9</sup> took into account the CR effects by applying the dynamic tube dilution (DTD) hypothesis<sup>10</sup> where the relaxed arm segments are considered to work as an effective solvent for the unrelaxed materials. Milner and McLeish further improved this theory by including the contributions of fast Rouse fluctuations at early times and solving the first-passage problem of a diffusing end monomer to retract a fractional distance  $s$  to get the arm relaxation spectrum  $\tau(s)$  at late times.<sup>4,5</sup> The Milner-McLeish theory predicts the stress relaxation of symmetric star polymer melts reasonably well, but not the dielectric or arm end-to-end vector relaxation function. It also encounters difficulty in using a single set of model parameters to describe the rheological behaviors of asymmetric star polymers with different short arm lengths.<sup>11</sup> In recent years computational

60 models based on the framework of Milner-McLeish theory have been developed for describ-  
61 ing the linear viscoelasticity of branched polymers with arbitrary architectures and their  
62 general mixtures.<sup>12–16</sup> These models have been shown to provide predictions in reasonably  
63 good agreement with experimental data for a variety of systems, but are facing problems in  
64 describing the linear rheology of some simple mixtures, such as the star-linear blends, espe-  
65 cially at low fractions of star polymers.<sup>16,17</sup> Therefore more quantitative theories that can  
66 simultaneously predict different dynamic and rheological properties of entangled branched  
67 polymers are still highly desired. The development of such theories requires the analytical  
68 solution of the multi-dimensional FP problem of arm retraction.<sup>18</sup>

69 On the other hand, the coarse-grained slip-link or slip-spring (SS) simulation mod-  
70 els have demonstrated strong potential in describing dynamics and rheology of entangled  
71 polymers.<sup>19–28</sup> For example, the single-chain slip-spring model developed by Likhtman<sup>25</sup> can  
72 provide simulation results on multiple experimentally measurable observables, such as neu-  
73 tron spin echo, linear rheology, dielectric relaxation and diffusion. Using a limited number  
74 of fitting parameters, the predictions of this model match the results obtained from both ex-  
75 periments and molecular dynamics (MD) simulations on linear and symmetric star polymers  
76 very well.<sup>26,29–31</sup> The SS model serves as an intermediate between tube theory and MD sim-  
77 ulations. As a discrete model, it not only naturally builds in all the relaxation mechanisms  
78 of the tube model, but also carries more system details, such as explicit polymer chains and  
79 entanglements<sup>32</sup>. At a higher level of coarse-graining, the SS model is significantly more  
80 efficient than MD simulations using bead-spring polymer model, which is of great advantage  
81 in the study of branched polymers. Furthermore, the slip-spring model can separate the con-  
82 tributions from different relaxation mechanisms by enabling some of them while disabling  
83 others. This is particularly helpful for examining assumptions made in current theoretical  
84 models and providing valuable information for developing more quantitative models. One  
85 typical application is to evaluate the magnitude of constraint release effects by comparing  
86 simulation results obtained from entangled polymer systems with and without CR.

87 Since deep arm retractions are rare events due to the high entropic barrier, the time and  
88 length scales accessible to standard slip-spring simulations are still much shorter than those  
89 in well-entangled experimental systems where the tube models are supposed to work best.  
90 Similar problems have also been seen in brute force simulations of many other rare events,  
91 such as crystal nucleation<sup>33,34</sup>, biological switches<sup>35</sup> and protein folding<sup>36</sup>. The required

92 computational time may take up to several decades.<sup>37</sup> Advanced numerical techniques, such  
93 as the umbrella sampling<sup>38</sup> and transition path sampling<sup>39</sup> methods, have to be employed  
94 to accelerate the simulations. Recently the forwards flux sampling (FFS) method has been  
95 proposed<sup>35,40,41</sup> and proven to be successful in molecular dynamics and Monte Carlo (MC)  
96 studies of rare events.<sup>37,42</sup>

97 In this work, we will combine the FFS method with the slip-spring model for studying  
98 the dynamics of entangled symmetric star polymers. This is a proof-of-concept work. To  
99 our knowledge the only reported work on applying the transition path sampling methods to  
100 study entanglement dynamics is the FFS simulation of Rouse chains in the regime relevant to  
101 arm retraction dynamics.<sup>18</sup> We will mainly focus on the systems without constraint release  
102 for the following reasons: 1) It is relatively convenient to implement the FFS method and  
103 find an appropriate reaction coordinate in the non-CR systems; 2) The terminal relaxation  
104 times in the systems without CR are much longer than those with CR, allowing us to  
105 test the computational efficiency and limit of the combined method; 3) Reliable simulation  
106 data on the FP times of arm retractions without CR are highly desired for examining  
107 analytical solutions of the multiple-dimensional Kramers problem<sup>18</sup>; 4) The extension of the  
108 method developed in the non-CR case to the CR case is fairly straightforward, as will be  
109 shown in Section V. With an optimized selection of the reaction coordinate, which is the  
110 index of the monomer that the innermost slip-link sits on, we first validate the proposed  
111 simulation method by producing simulation results on the terminal relaxation times  $\tau_d$  of  
112 mildly entangled star arms up to 8 entanglements in good agreement with those obtained  
113 from SS model simulations. The FFS simulations are then extended to longer arms with  
114 lengths up to 16 entanglements and so reach  $\tau_d$  values about 6 decades beyond that accessible  
115 by brute force simulations (from  $6 \times 10^6$  to  $3 \times 10^{12}$  SS unit time). The FP times of other  
116 original slip-links along the arm can be calculated using similar FFS simulations as for  
117 the innermost one, which consequently provides the entire arm relaxation spectrum  $\tau(s)$ .  
118 Moreover, we propose a numerical route to construct the arm end-to-end vector correlation  
119 functions,  $\Phi(t)$ , and stress relaxation functions,  $G(t)$ , from the discrete data stored at each  
120 interface during the FFS runs. Such time correlation functions are still not widely addressed  
121 in the FFS studies, but some relevant discussions could be found in the literatures for  
122 the FFS<sup>43,44</sup> and weighted ensemble methods.<sup>45-47</sup> Our simulation results will contribute to  
123 the development of theoretical models for describing the dynamics of entangled branched

124 polymers and also the general first-passage problems in multi-dimensional systems. The  
 125 simulation methodology developed in this work should also be applicable to the study of  
 126 rare events in other scientific areas.

127 The rest of this paper is organized as follows. In Section II, we introduce the single-chain  
 128 slip-spring model for entangled star polymers in the absence of CR. The detailed description  
 129 of the combined FFS and SS model is given in Section III. The simulation results obtained  
 130 in the non-CR systems are presented and discussed in Section IV, including the terminal  
 131 relaxation times  $\tau_d$ , the arm retraction spectra  $\tau(s)$  and the numerical route for constructing  
 132  $\Phi(t)$  and  $G(t)$ . In Section V, the simulation method is extended to study the arm retraction  
 133 dynamics of star polymers in the presence of CR. We draw conclusions in Section VI.

## 134 II. SLIP-SPRING MODEL FOR ENTANGLED SYMMETRIC STAR 135 POLYMERS

### 136 A. Model Description

137 In the single-chain slip-spring model for entangled symmetric stars, each star arm is  
 138 represented by a Rouse chain with  $N + 1$  monomers linked by  $N$  harmonic springs,<sup>25,48</sup> as  
 139 shown in Fig. 1. One end monomer with index 0 of the chain is treated as the branch point  
 140 which is fixed in space, while the other end with index  $N$  moves freely. The topological  
 141 constraints on the arm are modelled by a set of virtual springs each of  $N_s^{\text{SS}}$  beads. Each  
 142 virtual spring has one end connected to the Rouse chain by a slip-link that can slide along  
 143 the chain, and the other end, called anchor point, is fixed in space. The slip-spring model  
 144 effectively assumes a binary picture of entanglements, which is qualitatively supported by  
 145 recent MD simulation studies.<sup>49–51</sup> There is on average one slip-spring every  $N_e^{\text{SS}}$  monomers.  
 146 The values of  $N_e^{\text{SS}}$  and  $N_s^{\text{SS}}$  are adjustable for describing the intensity of entanglements. It  
 147 should be noted that  $N_e^{\text{SS}}$  is not necessarily equal to the entanglement length  $N_e$  used in  
 148 tube theory. Their relation will be discussed in Sec. IV B. To be consistent with previous  
 149 publications,<sup>25,30</sup> we choose  $N_e^{\text{SS}} = 4$  and  $N_s^{\text{SS}} = 0.5$ . Other parameters, such as the bead  
 150 friction coefficient  $\zeta_0$ , the average bond length  $b$  of the Rouse chain, the temperature  $k_B T$   
 151 and consequently the time scale  $\tau_0 = \xi_0 b^2 / k_B T$ , are all set to unity.

152 The Hamiltonian of the SS model is determined by the potential energies of both the

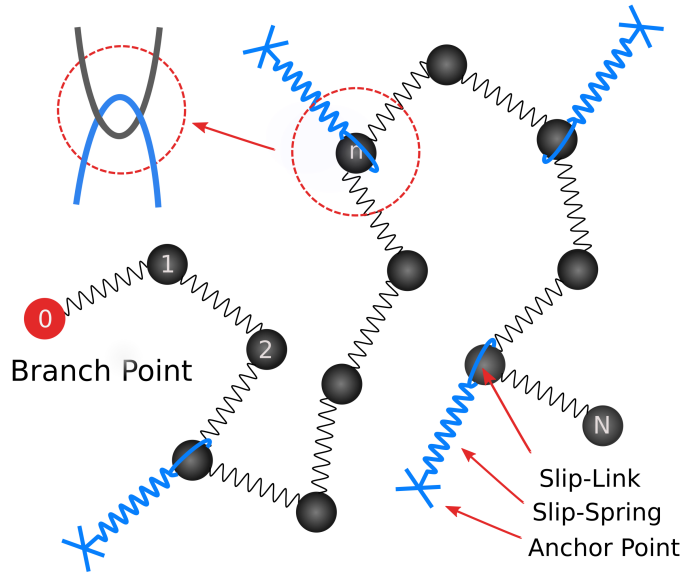


FIG. 1. Sketch of the single-chain slip-spring model for one arm of a symmetric star. The end monomer 0 represents the branch point which is fixed in space.

153 harmonic bonds of the Rouse chains and the virtual springs. The trajectories of the Rouse  
 154 monomers are obtained by solving their Langevin equations of motion numerically using an  
 155 integration time step size of  $\Delta t = 0.05\tau_0$ . In the original slip-spring model,<sup>25,29,30</sup> the slip-  
 156 links are assumed to travel continuously along the straight lines between adjacent monomers  
 157 and so can sit anywhere on the chain. In a later version of this model,<sup>31</sup> the slip-links  
 158 move discretely by hopping from one monomer to one of its nearest neighbors with the  
 159 acceptance rate controlled by a Metropolis Monte Carlo (MC) algorithm. The long-time  
 160 behavior of the system is not sensitive to the details of the slip-link motion. For simplicity  
 161 and computational efficiency, we employ the discrete motion approach in the current work.  
 162 One Monte Carlo hopping motion is attempted on average per slip-link at each time step.  
 163 It has been found recently by Shivokhin et al. that the slip-springs themselves could make  
 164 non-negligible contributions to the effective friction experienced by the Rouse chain when  
 165 moving along the tube, because the virtual springs with finite spring constant effectively  
 166 restrict the excursion volumes of the slip-links and so reduce their successful rate to hop  
 167 onto adjacent monomers.<sup>52</sup> As a consequence, an effective monomeric friction coefficient,  
 168  $\xi_{eff}(> \xi_0)$ , should be used instead of  $\xi_0$  when mapping the simulation results of the slip-



169 spring model to experimental data. But a constant change in the  $\xi$  value will not affect the  
170 discussions in this work, as all the data analysis and comparison are carried out within the  
171 slip-spring model framework. The effect of slip-link friction could be reduced by increasing  
172 the number of MC hopping attempts per time step at the price of higher computational cost.  
173 The slip-links are not allowed to sit on or pass through the branch points of the star arms.  
174 In the systems without constraint release, such as star polymers in a fixed polymer network,  
175 the destruction and creation of slip-links can only take place at the free ends of the star  
176 arms. Different from the systems with CR,<sup>25</sup> the slip-links are not coupled with each other.  
177 In addition, the slip-links on the same arm are not allowed to pass over each other or occupy  
178 the same monomer. This assumption introduces an effective excluded volume interaction  
179 between the slip-links, which is consistent with the low swapping rate between neighboring  
180 entanglements as revealed in a recent MD simulation of symmetric star polymer melts.<sup>51</sup>

181 The previous slip-spring simulations were typically carried out in an ensemble of chains  
182 and the total number of slip-links in the system is kept constant.<sup>25</sup> In the non-CR case,  
183 when one slip-link is deleted from a chain end, another slip-link will be added to the end of  
184 a randomly selected chain in the ensemble. For convenient installation of the FFS method,  
185 we modify the SS model for the non-CR case by simulating each entangled arm individually.  
186 The destruction of slip-links on a given arm is still incurred by the retraction of the arm  
187 free end (monomer index  $N$ ), but the addition of new slip-links to the same arm end is now  
188 determined by a probability  $P_{\text{add}}$  which satisfies the detailed balance condition

$$(1 - \rho_{\text{sl}}) (P_{\text{add}} + \rho_{\text{sl}} P_{N-1,N}) = \rho_{\text{sl}} (P_{\text{loss}} + (1 - \rho_{\text{sl}}) P_{N,N-1}), \quad (1)$$

189 where  $\rho_{\text{sl}} = 1/N_e^{\text{SS}}$  is the average number of slip-links sitting on each monomer.  $P_{i,j}$  is the  
190 transition probability for a slip-link to move from monomer  $i$  to monomer  $j$  and  $P_{\text{loss}}$  is the  
191 probability for a slip-spring sitting on the arm free end to be destructed after one integration  
192 time step, respectively. Eq. 1 thus represents the balance between the flux of slip-links to  
193 and from the end monomer. Assuming  $P_{N-1,N} = P_{N,N-1}$  without loss of generality, Eq. 1  
194 gives  $P_{\text{add}} \approx 0.167$  for the system parameters  $N_e^{\text{SS}} = 4$  and  $P_{\text{loss}} = 0.5$ . The modified SS  
195 model is validated by studying the static properties of the simulation system.

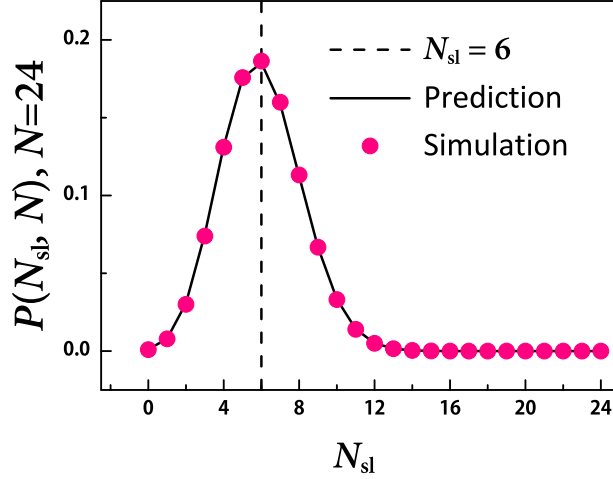


FIG. 2. Slip-spring model simulation results (circles) and predictions of Eq. 2 (line) on the probability distribution of number of slip-links per arm,  $P(N_{\text{sl}}, N)$ , for symmetric star polymers with arm length  $N = 24$ .

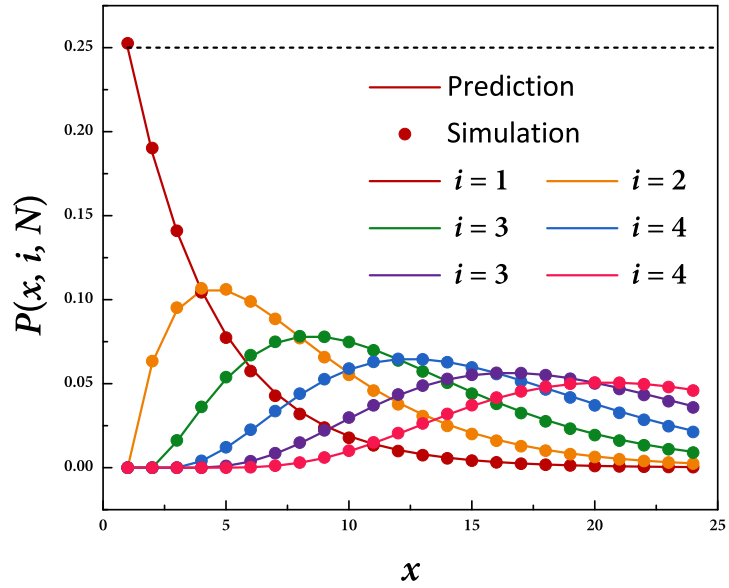


FIG. 3. Slip-spring model simulation results (symbols) and predictions of Eq. 4 (lines) on the probabilities of finding  $i$ -th slip-link on monomer  $x$ ,  $P(x, i, N)$ , for the symmetric star polymers with arm length  $N = 24$ . The horizontal dashed line shows the simulation results on the average number of slip-links found on each individual monomer.

196 **B. Static Properties**

197 The static property of the slip-spring model system of entangled symmetric star polymers  
 198 can be well characterized by the distribution of slip-links along the star arms. Considering  
 199 the effective excluded volume interactions between the slip-links, the problem is similar to  
 200 one-dimensional real gas in equilibrium. The probability distribution of finding  $N_{\text{sl}}$  slip-links  
 201 on a star arm of  $N$  monomers is simply given by

$$P(N_{\text{sl}}, N) = C_N^{N_{\text{sl}}} \rho_{\text{sl}}^{N_{\text{sl}}} (1 - \rho_{\text{sl}})^{N - N_{\text{sl}}}, \quad (2)$$

202 where  $C_N^{N_{\text{sl}}} = \frac{N!}{N_{\text{sl}}!(N - N_{\text{sl}})!}$ . Fig. 2 shows the good agreement between the prediction of  
 203 Eq. 2 and the SS model simulation results on  $P(N_{\text{sl}}, N)$  for the system with  $N = 24$ . It  
 204 can be seen that the peak value of  $N_{\text{sl}}$  is located at  $N_{\text{sl}} = 6$  in consistence with the expected  
 205 average number of slip-links per arm,  $\langle N_{\text{sl}} \rangle = \rho_{\text{sl}} N = 6$ .

206 When there are  $N_{\text{sl}}$  slip-links on a given arm, the probability to find the  $i$ -th slip-link on  
 207 the monomer  $x$  is

$$P(x, i, N_{\text{sl}}, N) = \frac{C_{x-1}^{i-1} C_{N-x}^{N_{\text{sl}}-i}}{C_N^{N_{\text{sl}}}}, \quad (i \leq x \leq N - N_{\text{sl}} + i) \quad (3)$$

208 where the numerator is a product of the possibilities to find  $i - 1$  slip-links on the arm  
 209 segment from monomer 1 to  $x - 1$  and to find  $N_{\text{sl}} - i$  slip-links on another segment from  
 210 monomer  $x + 1$  to  $N$ . It should be noted that in the star polymer systems without CR  
 211 the slip-links do not change their ordering along the star arms. In Eq. 3 the index  $i$  is  
 212 considered to increase from 1 for the innermost slip-link to higher values toward the arm  
 213 free end. Combining Eqs. 2 and 3, we obtain the ensemble-averaged probability to find the  
 214  $i$ -th slip-link on the monomer  $x$ :

$$P(x, i, N) = \sum_{N_{\text{sl}}=1}^N P(x, i, N_{\text{sl}}, N) P(N_{\text{sl}}, N). \quad (4)$$

215 Derivations of probability distributions similar to Eqs. 2 - 4 can also be found in a previous  
 216 work of Schieber.<sup>53</sup>

217 Fig. 3 presents the SS simulation results on  $P(x, i, N)$  for the slip-links with indices  
 218  $i = 1$  to 6 on star arms of length  $N = 24$ , together with the predictions of Eq. 4. The  
 219 good agreement between the two sets of data indicates that the simulation systems are  
 220 in equilibrium state and the randomly assigned locations of the anchor points can well

221 preserve the equilibrium distribution of the slip-links. This is also reflected by the fact that  
222 the average number of slip-links found on each individual monomer is equal to  $\rho_{sl} = 0.25$ ,  
223 see the horizontal line in Fig. 3.

### 224 III. COMBINED FFS AND SS METHOD FOR ENTANGLED STAR 225 POLYMERS WITHOUT CR

226 In the systems without CR, the topological constraints or entanglements imposed on a  
227 target arm are released hierarchically by the retraction of the arm free end. The terminal  
228 relaxation time  $\tau_d$  of the system is defined as the average first-passage time that takes the  
229 free end of an arm to reach the branch point starting from a random initial conformation.  
230 For well-entangled star arms,  $\tau_d$  grows exponentially with the number of entanglements per  
231 arm,  $Z$ .<sup>8</sup> However, full arm retraction rarely happens at large  $Z$  and so is generally not  
232 accessible by standard brute force simulations. There is also no exact analytical solution of  
233 this multi-dimensional FP problem. Therefore the forward flux sampling method introduced  
234 in Ref.<sup>35</sup> is employed in order to study these rare events. A successful application of the  
235 FFS method on studying the FP time of 1D Rouse chain with one fixed end can be found  
236 in Ref.<sup>18</sup>.

#### 237 A. Forward Flux Sampling Method

238 In FFS the phase space is divided by a sequence of non-crossing interfaces denoted by  $\lambda_i$   
239 ( $i = 0, \dots, m$ ), as sketched in Fig. 4(a). The starting states of the dynamic process are on  
240 the first interface  $\lambda_0$ , and the reactive or terminal states are on the last interface  $\lambda_m$ . These  
241 interfaces are defined by a reaction coordinate, which can be any parameter evolving during  
242 the process, but different choices could result in significantly different performance. More  
243 detailed discussion about the reaction coordinate is given in Sec. III B.

244 The FFS method is operated in two stages. In the first stage, a very long continuous  
245 simulation is performed in order to calculate the frequency  $\mu_0$  at which the trajectory crosses  
246 the interfaces  $\lambda_0$  and  $\lambda_1$  in sequence. In the second stage, a set of consecutive shooting  
247 simulations are carried out from interface  $\lambda_i$  to interface  $\lambda_{i+1}$  for  $i = 1, \dots, m - 1$ , which  
248 provide the transition probabilities  $P(\lambda_{i+1}|\lambda_i)$  that a system starting from  $\lambda_i$  will first reach

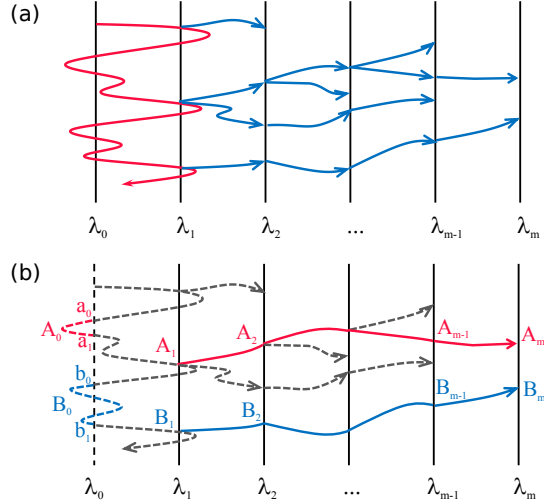


FIG. 4. (a) Schematic diagram of the FFS method. The continuous red trajectory is the continuous simulation in the first stage, and the blue trajectories are the successful shooting simulations in the second stage; (b) Algorithm for building continuous arm relaxation pathways from the piecewise shooting trajectories shown in (a).

249  $\lambda_{i+1}$  rather than return to  $\lambda_0$ . The first-passage time  $\tau_n$  for the system starting from the  
 250 first interface  $\lambda_0$  and ending on the interface  $\lambda_n$  ( $1 \ll n \leq m$ ), is then given by

$$\tau_n = \frac{1}{\mu_0 \prod_{i=1}^{n-1} P(\lambda_{i+1}|\lambda_i)}, \quad 1 \ll n \leq m \quad (5)$$

## 251 B. Reaction Coordinate

252 A key issue in applying the FFS method is the choice of the reaction coordinate. Starting  
 253 from a random initial configuration, the relaxation of a star arm in the system without CR  
 254 proceeds by the retraction of the arm free end along the primitive path, passing through  
 255 all the original slip-links on the arm sequentially until none left between it and the branch  
 256 point. The terminal relaxation time is determined by the moment at which the innermost  
 257 slip-link is released. During this process, the number of surviving original slip-links,  $N_{sl}$ , on  
 258 the arm drops with time from its initial value to 0, making it an intuitively simple choice for  
 259 the reaction coordinate. Considering that the value of  $N_{sl}$  is statistically proportional to the  
 260 length of the surviving tube or primitive path, this choice would be consistent with a recent  
 261 FFS study on the FP time for the free end of a 1D Rouse chain to reach a certain distance  
 262  $z$  from the fixed end where  $z$  was selected as the reactive coordinate.<sup>18</sup> The 1D Rouse chain

263 study is closely related to the current work, because arm extension is essentially the reverse  
 264 process of arm retraction. However, when using  $N_{sl}$  as the reaction coordinate, our FFS  
 265 simulation results on the terminal arm retraction times are found to be significantly smaller  
 266 than those obtained from standard SS model simulations. The problem arises from the  
 267 difficulty in choosing equivalent starting states for the FFS runs. In the slip-spring model  
 268 system, both the instantaneous number of slip-links and their distribution along the arm  
 269 are subject to strong fluctuations, especially on the outer arm segments which undergo fast  
 270 Rouse motion. In the FFS runs using  $N_{sl}$  as the reaction coordinate, the starting states are  
 271 collected in the first-stage continuous simulation as the configurations where the number  
 272 of slip-links on the arm is equal to the ensemble-averaged value of  $\langle N_{sl} \rangle = N\rho_{sl}$ . Shooting  
 273 from these starting configurations, only the samples in which the values of  $N_{sl}$  decrease  
 274 monotonically are considered to reach interface  $\lambda_1$  successfully. This biased strategy is thus  
 275 in favor of the samples where the initial slip-link densities on the outer arm segments are  
 276 higher than  $\rho_{sl}$ , because in such cases the probability to lose slip-links at short times is  
 277 higher than to gain ones. Therefore a relatively large proportion of slip-links on a sample  
 278 arm are released by shallow arm retractions at early times, leaving fewer than the average  
 279 number of slip-links on the surviving segments of the primitive path. As a consequence, the  
 280 terminal relaxation times obtained from the FFS simulations are shorter than those obtained  
 281 from standard SS simulations where the ensemble-averaged initial distribution of slip-links  
 282 is uniform. These results imply that the reaction coordinate should be selected close to the  
 283 branch point in order to minimize the influence of the fast fluctuating arm end.

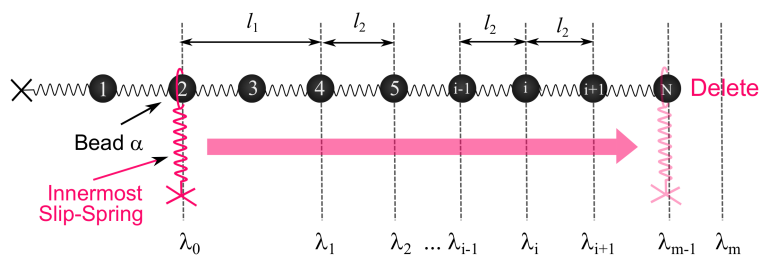


FIG. 5. Application of FFS method for studying the retraction dynamics of an entangled star arm described by the slip-spring model. The cross (Monomer 0) on the left represents the branch point that is fixed in space. The interfaces  $\lambda_i$  (vertical lines) used in the FFS simulations are placed on the monomers of the arm.

284 Since the terminal arm relaxation time is determined by the release of the innermost

285 slip-link from the arm free end, one can track the motion of this particular slip-link along  
 286 the arm by defining the index of the monomer that it sits on as the reaction coordinate.  
 287 As shown in Fig. 5 where the 3D Rouse chain is sketched as a straight line for convenience  
 288 of discussion, the first interface  $\lambda_0$  used in FFS is set on monomer  $\alpha$  (2 in this case) where  
 289 the innermost slip-link originally sits on. Any initial configuration of the confined arm in  
 290 which the innermost slip-link locates on monomer  $\alpha$  can be taken as the starting state of  
 291 the FFS simulation. The second last interface  $\lambda_{m-1}$  is placed on the outermost monomer  $N$   
 292 of the arm, and the last interface  $\lambda_m$  is right outside of the arm free end, marking the final  
 293 or reactive state that the arm free end has passed through the innermost slip-link and the  
 294 arm is fully relaxed. The other  $m - 2$  interfaces are placed on the monomers in between  $\alpha$   
 295 and  $N$ .

296 According to the standard FFS method, a database containing a large number of configura-  
 297 tions is accumulated on each interface. In the first stage of the continuous simulation, the  
 298 database on  $\lambda_1$  is a collection of configurations whose innermost slip-link lastly crossed  $\lambda_0$   
 299 before crossing  $\lambda_1$ . In the second stage, consecutive shooting simulations are performed from  
 300 interface  $\lambda_i$  to  $\lambda_{i+1}$ ,  $i = 1, \dots, m - 1$  using starting configurations randomly selected from  
 301 the database on  $\lambda_i$ . Among the  $M_i$  shooting samples, the ones whose innermost slip-links  
 302 reach  $\lambda_{i+1}$  before going back to  $\lambda_0$  are considered as successful samples and will be stored  
 303 in the database of  $\lambda_{i+1}$ .

### 304 C. Simulation Details

305 Apart from the reaction coordinate, the performance of the FFS algorithm can also be  
 306 affected by some other factors. One factor is that the configurations saved in the database  
 307 of interface  $\lambda_1$  during the first-stage continuous simulation could be strongly correlated with  
 308 each other due to the limited running time at this stage in comparison with  $\tau_d$ . This may  
 309 introduce systematic errors in the simulation results if the size of the database is fixed.  
 310 This problem can be resolved by increasing the interval  $l_1$  between the interfaces  $\lambda_0$  and  
 311  $\lambda_1$ , as shown in Fig. 5, and recording configurations on  $\lambda_1$  at a lower frequency  $\omega$ . For  
 312 example, rather than recording every event that the innermost slip-link crosses  $\lambda_1$  when  
 313 coming from  $\lambda_0$ , one can record once for every  $1/\omega$  crossings. Another factor is the choices  
 314 of the interface interval  $l_2$  between  $\lambda_i$  and  $\lambda_{i+1}$  ( $i = 1, \dots, m - 2$ ) and the number of shooting

315 samples  $M_i$  from each  $\lambda_i$  which determine the performance of the FFS in the second stage.  
 316 Since  $l_2$  controls the transition probabilities  $P(\lambda_{i+1}|\lambda_i)$ , a smaller  $l_2$  is normally preferred  
 317 for accelerating the shooting simulations. The number  $M_i$  can then be chosen according to  
 318  $P(\lambda_{i+1}|\lambda_i)$  and the desired accuracy.

319 In the current work, we take  $l_1 = 2$  and  $l_2 = 1$  which separate the first two interfaces  
 320  $\lambda_0$  and  $\lambda_1$  by one bead and then set one interface on every bead along the arm. The  
 321 recording frequency  $\omega$  has to be reduced for longer arms in order to reduce the conformational  
 322 correlations on  $\lambda_1$  and is empirically taken to be  $\omega = 1/(N - 15)$  for arm length  $N \geq 16$ .  
 323 Since the reaction coordinate is defined by the location of the innermost original slip-link,  
 324 the transition probability  $P(\lambda_{i+1}|\lambda_i)$  increases with  $i$  towards the arm free end. In order to  
 325 achieve good statistics for the first few interfaces close to the branch point,  $M_i$  should be  
 326 large enough. A number of samples  $M_i = 40,000$  is thus used for  $\lambda_i, i = 1, 2, \dots, m - 1$  in all  
 327 of the FFS simulation runs. As shown in Fig. 3, there is a non-negligible fraction of initial  
 328 configurations where the innermost slip-links are many monomers away from the branch  
 329 point and could be released by shallow arm retractions. The terminal relaxation times of  
 330 such arms are thus much shorter than those of the arms with uniform slip-link distributions.  
 331 Actually, their terminal times have been reached in the first-stage continuous simulations  
 332 without going into the second stage of FFS. These  $\tau_d$  data are still counted for calculating  
 333 the distribution and the mean value of the terminal relaxation times.

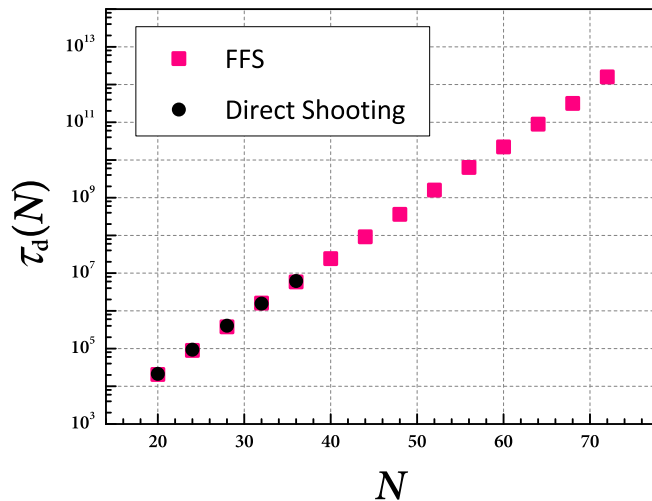


FIG. 6. Simulation results on the terminal arm retraction time  $\tau_d$  obtained from FFS and direct shooting simulations as a function of arm length  $N$ .



## 334 IV. RESULTS AND DISCUSSIONS FOR SYSTEMS WITHOUT 335 CONSTRAINT RELEASE

### 336 A. Terminal Time of Arm Retraction

337 The terminal time  $\tau_d$  of the arm retraction process is the main and most straightforward  
338 output of the FFS simulations. Fig. 6 presents the FFS results on  $\tau_d$  as a function of  
339 the arm length  $N$ . For comparison, we have also included the  $\tau_d$  data obtained from the  
340 so-called direct shooting simulations which start from the first interface  $\lambda_0$  and stop at the  
341 last interface  $\lambda_m$  without intermediate steps. These runs are equivalent to the slip-spring  
342 simulations using initial configurations randomly picked from the database on interface  $\lambda_0$   
343 and running continuously until the innermost original slip-spring being deleted by the arm  
344 free end. For each arm length, the direct shooting simulation results are averaged over 10,000  
345 independent samples, while in the FFS simulations  $\tau_d$  is averaged over 2,000 independent  
346 runs. Since in each FFS run, there are 40,000 samples recorded on  $\lambda_1$ , the average is actually  
347 taken over a much bigger ensemble than that of the direct shooting runs. Considering the  
348 high computational cost, the direct shooting simulations are only performed for arm lengths  
349 from  $N = 20$  to 36, corresponding to about 4 to 8 entanglements per arm estimated with  
350  $N_e \approx 4.47$  as discussed in Sec. IV B. In this range of  $N$ , the FFS and direct shoot simulation  
351 results in Fig. 6 show very good agreement with the relative differences less than 5%. The  
352 combined FFS and SS method and the choice of the reaction coordinate are thus well  
353 justified.

354 Fig. 7 compares the average computational times required to complete a single direct  
355 shooting and a single FFS run on a single CPU (Intel Xeon E5-2620). The direct shooting  
356 simulation is faster at short arm lengths, but its computational time grows exponentially  
357 with  $N$  and overtakes that of the FFS when  $N \geq 32$ . The FFS method allows us to study  
358 much longer arms. For entangled star polymers with arm length  $N = 72$  in the absence of  
359 CR, the terminal relaxation time is found to be  $\tau_d \approx 2.85 \times 10^{12}$  which is about 8 orders  
360 of magnitude longer than that of stars with  $N = 20$  and is hardly accessible to any type of  
361 direct simulations unless running on a supercomputer for several years.

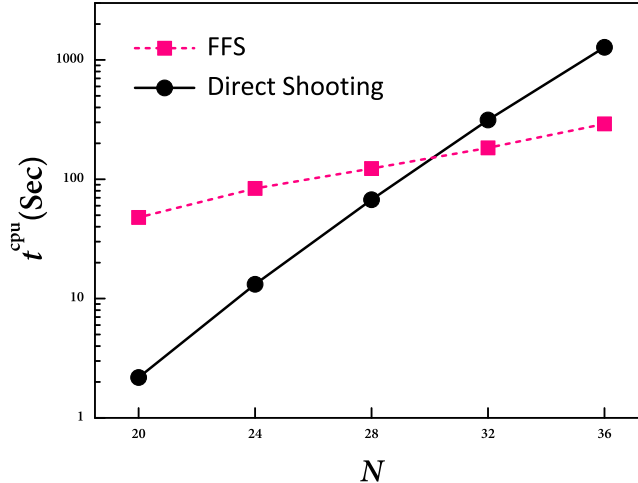


FIG. 7. Average computational times required for completing a single FFS and a single direct shooting run on a single Intel Xeon processor.

## 362 B. Comparison with Theoretical Model Predictions

363 The  $\tau_d$  data in Fig. 6 show a clear exponential dependence on the arm length  $N$ , which is  
 364 expected from the Pearson-Helfand theory for star arms retracting in a fixed network.<sup>8</sup> These  
 365 results can be further compared with the predictions of more detailed theoretical models.<sup>4,5,18</sup>  
 366 The Milner-McLeish theory based on the solution of 1D Kramers problem predicts the  
 367 terminal arm retraction time in the absence of CR as<sup>4,5</sup>

$$\tau_d(N) = \frac{\pi^{5/2}}{4\sqrt{6}} \tau_R(N) \frac{1}{z} \exp\left(\frac{3z^2}{2}\right), \quad (6)$$

368 where  $z = \sqrt{N/N_e}$  and the arm Rouse time  $\tau_R(N) = 4\zeta_0 N^2 b^2 / 3\pi^2 k_B T$ . The entanglement  
 369 molecular weight  $N_e$  can be estimated by substituting the corresponding FFS result on  $\tau_d(N)$   
 370 into Eq. 6. As shown in Fig. 8, the obtained  $N_e$  values are roughly independent of  $N$ , giving  
 371  $N_e \approx 4.94$ .

372 Recently Cao et al. pointed out that the first-passage problem of Rouse chain should  
 373 be treated as a multi-dimensional Kramers problem.<sup>18</sup> FFS simulations of 1D Rouse chains  
 374 showed that the  $z^{-1}$  scaling in the prefactor of  $\tau_d$  as predicted in Eq. 6 is only valid for very  
 375 large chain extensions. In the intermediate chain extension regime corresponding to realistic  
 376 arm retraction process, a new theory based on the Freidlin-Wentzell theory was proposed,<sup>54</sup>

377 which predicts a  $z^{-3}$  scaling in the prefactor of the terminal time [Eq. 60 in Ref.<sup>18</sup>]

$$\tau_d(N) = \frac{C(N)\tau_R(N)}{z^3} \exp\left(\frac{3z^2}{2}\right), \quad (7)$$

378 where  $C(N)$  is a fitting parameter. For arm lengths  $N \geq 20$  we can take the plateau value of  
 379  $C(N) = 1.2$  as found in the FFS simulations of 1D Rouse chains.<sup>18</sup> The  $N_e$  values calculated  
 380 by substituting the FFS data on  $\tau_d(N)$  into Eq. 7 are shown in Fig. 8, which increase with  
 381 the increasing arm-length and approach an asymptotic value of  $N_e \approx 4.47$  that is smaller  
 382 than the  $N_e$  value estimated by using Eq. 6. The two theoretical models thus predict  
 383 qualitatively different dependence of  $N_e$  on  $N$ , at least in the systems without CR. Since  
 384 the entanglement molecular weight is one of the most important model input parameters  
 385 for predicting the dynamics and rheology of entangled polymers, this  $N$ -dependent behavior  
 386 apparently needs further investigation for developing quantitative theories. The FFS results  
 387 on  $\tau_d$  over a broad range of arm lengths should work as a benchmark for examining theoretical  
 388 models that are typically developed for well-entangled polymers.

389 In Eqs. 6 and 7, the parameter  $\nu$  used in the quadratic arm retraction potential is taken to  
 390 be  $3/2$  as originally proposed by Doi and Edwards for describing contour length fluctuations  
 391 or arm retractions in a fixed network.<sup>2</sup> But computer simulation and theoretical works have  
 392 suggested that the value of  $\nu$  actually has an arm-length dependence and even the quadratic  
 393 form of the arm retraction potential may be subject to change once taking into account the  
 394 enthalpic contributions.<sup>55,56</sup> When we fit the  $\tau_d$  data in Fig. 6 to an exponential function  
 395 of  $\tau_d(N/N_e) = A \exp[\nu(N/N_e)]$  with  $N_e = 4.94$  over the whole range of arm length  $N$  we  
 396 studied, a value of  $\nu \approx 1.69$  is found, which is somewhat larger than  $3/2$ . On the other  
 397 hand, the theoretical predictions of Eq. 6 using  $\nu = 3/2$  and  $N_e = 4.94$  also agree with  
 398 the simulation data reasonably well. To examine the  $\nu$  parameter using Eq. 7 with a fixed  
 399  $N_e$  value could be more complicated, because this theoretical model was derived using the  
 400 constant value of  $\nu = 3/2$ . Considering that the simulation results in Fig. 6 are obtained  
 401 in the systems without CR and the slip-spring model does not involve explicit enthalpic  
 402 contributions, we keep  $\nu$  as a constant in the comparison with theoretical models in the  
 403 current work.

404 We note that the  $N_e$  values given in Fig. 8 are different from that obtained by mapping  
 405 the original slip-spring model simulation results on the linear viscoelastic properties of linear  
 406 polymer melts to the Likhtman-McLeish model predictions ( $N_e \approx 5.7$ ).<sup>25,30</sup> The difference

407 could be related to the use of different theoretical models for the data fitting, the presence of  
 408 constraint release effects in the polymer melts and the different ways of treating the slip-link  
 409 motion along the polymer chains, namely continuously or discretely, as discussed in Sec.  
 410 II A. The value of  $N_e \approx 4.94$  we found is very close to the value of  $N_e = 4.89$  estimated by  
 411 Shivokhin et al. for the slip-spring model using the same set of model parameters  $N_e^{SS} = 4$   
 412 and  $N_s^{SS} = 0.5$ .<sup>52</sup>

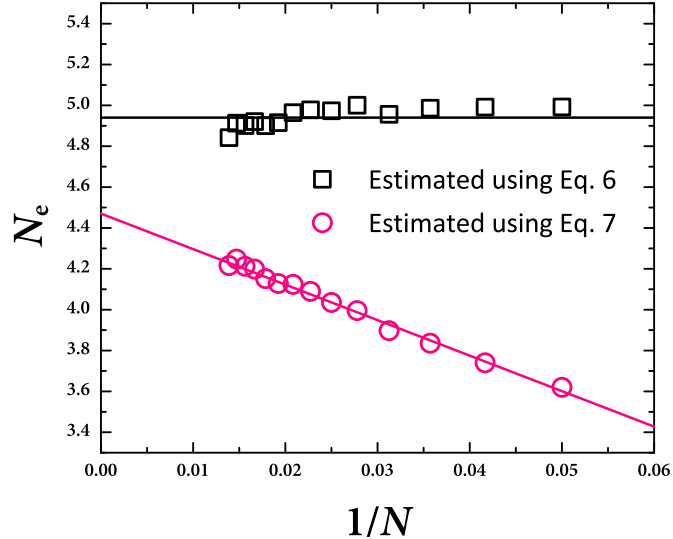


FIG. 8. Entanglement molecular weight  $N_e$  calculated by substituting the FFS simulation results on  $\tau_d$  (Fig. 6) into the theoretical predictions of Eqs. 6 (squares) and 7 (circles) for various arm lengths.

### 413 C. Arm Relaxation Spectrum

414 Apart from terminal relaxation time, the FFS method can also be applied to obtain the  
 415 entire relaxation spectrum of the arm. This is done in a similar way as calculating  $\tau_d$ . The  
 416 only difference is to set the index of the monomer that the  $i$ -th original slip-link sits on,  
 417 instead of that of the innermost slip-link, as the reaction coordinate. Accordingly, the first  
 418 interface  $\lambda_0$  in the FFS method is defined on the monomer where the  $i$ -th slip-link originally  
 419 occupied. The FP time of the  $i$ -th slip-link is recorded as  $\tau(X)$  with the fractional index  
 420  $X = i/\langle N_{sl} \rangle$ . The simulation results on  $\tau(X)$  are plotted in Fig. 9 for the arm lengths  
 421  $20 \leq N \leq 44$ . For the systems with  $N \leq 36$ , the direct shooting simulation results are

422 also presented for comparison. The agreement between the FFS and direct shooting data  
 423 gets improved as the arm free end retracts deeper along the primitive path, i.e., with the  
 424 decrease of the slip-link index  $i$  and so  $X$ . This is understandable because the release of  
 425 the outer slip-links or entanglements is dominated by the fast Rouse-like fluctuations. The  
 426 corresponding entropic barrier is relatively low such that the FFS method does not work well  
 427 at large  $X$ . For this reason, the most reliable relaxation spectrum, especially for the long  
 428 arms, should be constructed by combining the FP times of the inner slip-links as calculated  
 429 by the FFS method with the FP times of the outer ones obtained from direct shooting  
 430 simulations. One such example is shown in Fig. 9 for the systems with  $N = 44$ . The  
 431 complete relaxation spectrum  $\tau(X)$  can be directly applied to test theoretical models of arm  
 432 retraction dynamics.

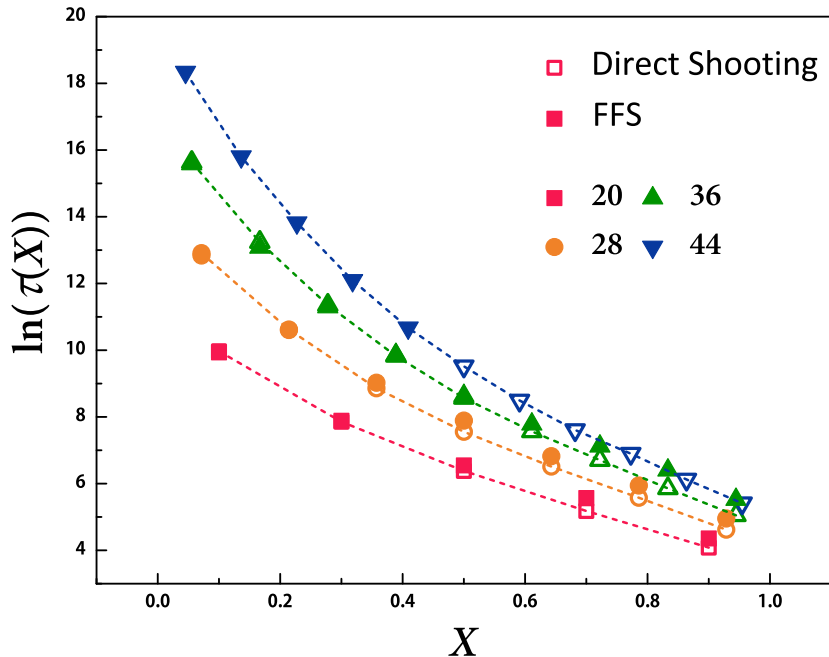


FIG. 9. Relaxation spectrum calculated using the first-passage times of all slip-links for star arms  
 with various lengths obtained by both FFS (solid symbols) and direct shooting (open symbols)  
 simulations. The dashed curves are for guiding the eye. The parameter  $X = i / \langle N_{sl} \rangle$  is the  
 fractional index of the  $i$ -th slip-link along the arm, which increases from  $X = 1 / \langle N_{sl} \rangle$  for the  
 innermost slip-link to  $1 - 1 / \langle N_{sl} \rangle$  for the outermost one.

## 433 D. Constructing Relaxation Correlation Functions

434 In experiments, the dynamics and rheology of entangled polymers are generally charac-  
435 terized by the dielectric relaxation or chain end-to-end vector correlation function,  $\Phi(t)$ , and  
436 the stress relaxation function,  $G(t)$ . The calculation of these observables usually requires the  
437 continuous trajectories of the polymers, which are however not naturally available in FFS  
438 simulations, because only instantaneous configurations at the hitting points on the interfaces  
439 are recorded. Here we introduce a numerical route to effectively link these discrete pieces  
440 of information to construct the dielectric and stress relaxation functions. The systems of  
441 entangled star polymers without CR are used as examples to demonstrate the application  
442 of this algorithm.

443 Fig. 4(b) sketches the method used to build continuous arm relaxation pathways from the  
444 piecewise FFS shooting trajectories shown in Fig. 4(a). Considering two hitting points on  
445 the terminal interface  $\lambda_m$ , marked as  $A_m$  and  $B_m$ , there must be two continuous trajectories  
446 or pathways that one can track back from them to the first interface  $\lambda_0$ . As shown in Fig.  
447 4(b), the pathway to state  $A_m$  is constructed by linking the successful shooting trajectory  
448 from the hitting point  $A_{m-1}$  to  $A_m$  with that from  $A_{m-2}$  to  $A_{m-1}$ , and so on until reaching  
449 the point  $A_1$  on the interface  $\lambda_1$ . The linking from  $A_1$  to a start point  $A_0$  is obtained  
450 from the trajectory generated in the continuous simulation in the first stage of the FFS  
451 simulations. Similarly, the pathway to the hitting point  $B_m$  can be traced back to  $B_1$  on  
452  $\lambda_1$  and then to a starting point  $B_0$ . We note that these rebuilt trajectories are different  
453 from the true continuous trajectories generated in standard slip-spring model simulations,  
454 but the ensemble-averaged pathways obtained in these two cases should be very close, as  
455 reflected in the consistent  $\Phi(t)$  and  $G(t)$  results in Fig. 11. From computational point  
456 view, the rebuilding method requires the storage of all the successful shooting trajectories  
457 between neighboring interfaces and also a large memory for data processing. This may limit  
458 its application to large systems such as the fine-grained bead-spring models widely used in  
459 molecular dynamics simulations.

460 When calculating the arm relaxation correlation functions from the rebuilt trajectories,  
461 two assumptions have been made. First, when one slip-link is destroyed by the retracting  
462 arm free end, the primitive path segment in between its nearest neighboring slip-link and  
463 itself will be forgotten immediately. This assumption is valid for most of the slip-links due to

464 the discrete feature of entanglements in the SS model. The only exception is with the tube  
465 segment between the branch point and the innermost slip-link where this assumption may  
466 affect the calculation of the relaxation functions, as discussed below. The second assump-  
467 tion is that the FP times on each interface follow a single exponential distribution. This  
468 assumption has also used in solving the 1D Kramers problem and in the Doi-Edwards tube  
469 model without CR.<sup>2</sup> Since the slip-spring model is essentially a multidimensional problem,  
470 we perform an extra set of simulations to examine the validity of this assumption. A total  
471 number of 10,000 direct shooting simulations, all starting from exactly the same initial con-  
472 figuration, are carried out to mimic a FFS run. The FP times for the innermost slip-link  
473 to reach different monomers, or different interfaces in the FFS definition, are recorded. Fig.  
474 10 presents the probability distributions,  $P_i(t)$ , of the FP times on three different interfaces  
475 for the arms of length  $N = 20$ . It can be seen that  $P_i(t)$  on interfaces with higher indexes  
476 can be well described by the exponential function

$$P_i(t) = \frac{1}{\tau_i} \exp\left(-\frac{t}{\tau_i}\right) \quad (8)$$

477 where  $\tau_i$  is the mean FP time on the interface  $\lambda_i$ . The second assumption becomes valid as  
478 the arm free end retracts deeply along the primitive path.

479 Following Eq. 8 the probability that the innermost slip-link has never crossed the interface  
480  $\lambda_i$  after time  $t$  is

$$P_{\lambda_0}^{\lambda_i}(t) = \exp\left(-\frac{t}{\tau_i}\right), \quad i = 1, 2, \dots, m \quad (9)$$

481 and the probability that it has crossed  $\lambda_i$  at least once is

$$P_{\lambda_i}^{\infty}(t) = 1 - \exp\left(-\frac{t}{\tau_i}\right), \quad i = 1, 2, \dots, m. \quad (10)$$

482 Therefore the probability that the trajectory starting from  $\lambda_0$  has crossed interface  $\lambda_i$  but  
483 never crossed interface  $\lambda_{i+1}$  is

$$P_{\lambda_i}^{\lambda_{i+1}}(t) = P_{\lambda_i}^{\infty}(t) - P_{\lambda_{i+1}}^{\infty}(t) = -\exp\left(-\frac{t}{\tau_i}\right) + \exp\left(-\frac{t}{\tau_{i+1}}\right), \quad i = 1, 2, \dots, m-1. \quad (11)$$

484 Using Eqs. 9, 10 and 11, the time correlation function of a dynamic observable,  $V$ , whose  
485 instantaneous values are calculated on different interfaces can be evaluated by

$$\langle V(t)V(0) \rangle = \left\langle P_{\lambda_0}^{\lambda_1}(t)W_0 + \sum_{i=1}^{m-1} P_{\lambda_i}^{\lambda_{i+1}}(t)W_i + P_{\lambda_m}^{\infty}(t)W_m \right\rangle \quad (12)$$

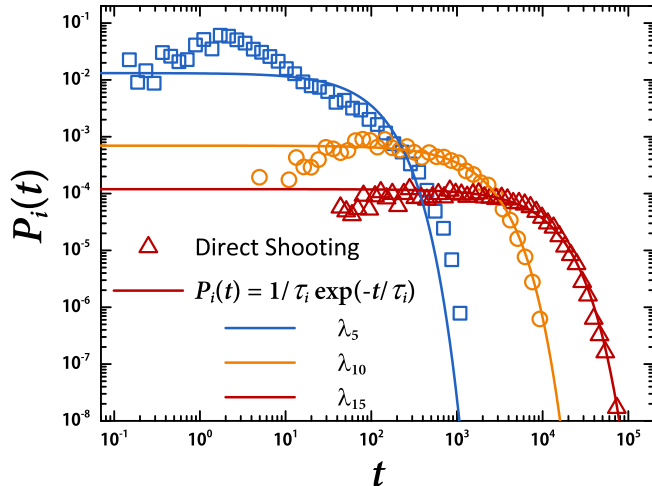


FIG. 10. Probability distributions of the first-passage times for the innermost slip-link to reach different monomers or different interfaces in the FFS definition  $\lambda_i$  along the arm as calculated by direct shooting slip-spring simulations of star arms of length  $N = 20$ . All of the 10,000 simulations start from the same initial configuration where the innermost slip-link sits on monomer 1 next to the branch point. The solid lines represent a single exponential fit to the simulation data in each case.

486 where  $W_i$  is defined as

$$W_i = \frac{1}{h_i} \sum_{k=1}^{h_i} V_i^k V_0^k, \quad i = 0, 1, \dots, m. \quad (13)$$

487 Here  $h_0$  is the number of starting points on the first interface  $\lambda_0$  and  $V_0^k$  is the observable  
 488 value at the  $k$ -th starting point. Similarly  $h_i$  ( $i = 1, \dots, m$ ) is the number of hitting points  
 489 on the interface  $\lambda_i$  out of the  $M_{i-1}$  shootings from  $\lambda_{i-1}$  and  $V_i^k$  is the observable value at  
 490 the  $k$ -th hitting point on  $\lambda_i$ , respectively. For the system sketched in Fig. 4(b), there are  
 491 only 2 hitting points on the final interface  $\lambda_m$  such that  $h_m = 2$  in Eq. 13.

492 Substituting Eqs. 10 and 11 into Eq. 12, we get

$$\langle V(t)V(0) \rangle = \left\langle \sum_{i=0}^{m-1} \Delta W_{i,i+1} \exp\left(-\frac{t}{\tau_{i+1}}\right) + W_m \right\rangle, \quad (14)$$

493 where  $\Delta W_{i,i+1} = W_i - W_{i+1}$ . The correlation function in Eq. 14 is expressed as a weighted  
 494 summation of a set of exponential functions, which is consistent with the tube model pre-  
 495 dictions for the end-to-end vector and stress relaxation functions of entangled polymers in  
 496 the absence of constraint release.<sup>2</sup> The only difference lies in the last term  $W_m$  on the right



497 hand side of Eq. 14 which, if being nonzero, may result in an unphysical plateau after the  
 498 terminal relaxation time  $\tau_d$ .

499 The problem associated with  $W_m$  does not exist in the tube model where the tube is  
 500 assumed to be continuous.<sup>2</sup> The arm free end can thus retract continuously along the prim-  
 501 itive path all the way to the branch point and so release all the memories in the original  
 502 tube. As a result,  $W_m$  equals to zero for all dynamic observables. However, in the slip-spring  
 503 model the entanglements are represented discretely by the slip-links. The terminal time  $\tau_d$   
 504 is taken to be the time when the arm free end passes the innermost slip-link. In standard  
 505 slip-spring model simulations, the memories, such as stress and arm end-to-end vector ori-  
 506 entation, stored in the original tube segment between the innermost slip-link and the branch  
 507 point can still be released by the continuous relaxation of the arm beyond  $\tau_d$ . But in the  
 508 FFS simulations, the runs are terminated right after  $\tau_d$  when the trajectories reach the last  
 509 interface  $\lambda_m$ . Although this termination does not affect the determination of the terminal  
 510 time as shown above, it artificially traps the unreleased memories in the last tube segment  
 511 in the configurations saved on  $\lambda_m$ , leading to a nonzero ensemble average value of  $W_m$ . As  
 512 an attempt to recover the full relaxation function, we propose a simple approximation to  
 513 incorporate the arm relaxation dynamics beyond the terminal time  $\tau_d$  ( $= \tau_m$ ), which is to  
 514 multiply the  $W_m$  term in Eq. 14 with an exponential time decay function, giving

$$\langle V(t)V(0) \rangle = \left\langle \sum_{i=0}^{m-1} \Delta W_{i,i+1} \exp\left(-\frac{t}{\tau_{i+1}}\right) + W_m \exp\left(-\frac{t}{\tau_m}\right) \right\rangle. \quad (15)$$

515 The dielectric and stress relaxation functions calculated using Eq. 15 from the rebuilt  
 516 trajectories are plotted in Fig. 11 for arm lengths up to  $N = 72$ . For comparison, the  $\Phi(t)$   
 517 and  $G(t)$  data obtained from standard slip-spring model simulations are also included for  
 518 the systems with  $N \leq 36$ . In these calculations, the dielectric or arm end-to-end vector  
 519 relaxation function is defined as  $\Phi(t) = \langle \mathbf{R}_e(t) \cdot \mathbf{R}_e(0) \rangle / \langle \mathbf{R}_e^2(0) \rangle$  where  $\mathbf{R}_e$  is the arm end-  
 520 to-end vector and the mean square end-to-end distance  $\langle \mathbf{R}_e^2(0) \rangle = Nb^2$ . The  $G(t)$  results  
 521 are the single-arm stress autocorrelation functions without considering the cross-correlation  
 522 contributions from the virtual springs.<sup>57,58</sup> This choice does not affect any discussions or  
 523 conclusions in the current work, especially when there is no constraint release effect. The  
 524  $\Phi(t)$  and  $G(t)$  results obtained by using the rebuilding method and from the standard SS  
 525 model simulations show reasonably good agreement in the terminal regime, indicating the  
 526 capability of Eq. 15 in constructing the arm relaxation functions using discrete FFS shooting

527 trajectories. The noticeable discrepancy between the two sets of data in each case at short  
 528 time scales could be attributed to the fact that the exponential distribution assumption  
 529 of the FP times does not apply to the first few interfaces, as shown in Fig. 10. On the  
 530 other hand, we have also applied Eq. 14 directly to construct the relaxation functions  
 531 of the systems with  $N = 36$ . The obtained  $\Phi(t)$  and  $G(t)$  curves (dashed lines) initially  
 532 coincide with those calculated using Eq. 15, but start to decay slower when some of the  
 533 sample trajectories have reached their terminal times and the constant  $W_m$  contributions  
 534 are counted in. The unphysical plateaus are reached after the mean terminal time  $\tau_d$  for the  
 535 reasons discussed above. Therefore at least for the combined FFS and SS method we used,  
 536 the algorithm for constructing the time correlation functions needs to take into account the  
 537 arm relaxation behavior beyond  $\tau_d$ .

## 538 **V. EXTENSION OF THE COMBINED FFS AND SS METHOD TO** 539 **SYSTEMS WITH CONSTRAINT RELEASE**

540 The combined FFS and SS method can be extended to entangled polymer systems with  
 541 CR by adjusting the definition of the reaction coordinate. In the standard slip-spring  
 542 model,<sup>25,51</sup> constraint release is included by coupling the slip-links sitting on different poly-  
 543 mer chains or arms into pairs to represent the binary entanglements. When one slip-link  
 544 is deleted from the free end of an arm, its coupled partner is also deleted regardless of its  
 545 location, which results in a CR event. This means that for FFS simulations the originally  
 546 innermost slip-link alone could not be used to define a reaction coordinate for exploring  
 547 the entire arm relaxation spectrum, because this slip-link may be destructed by a CR event  
 548 before reaching the arm free end. To resolve this problem, we refer to a recent slip-spring  
 549 simulation work on entangled symmetric star polymers with CR.<sup>51</sup> There it was shown that  
 550 the relaxation of the original tube segments, and correspondingly the relaxation of the arm  
 551 end-to-end vector, is dominated by the first-passage times of the so-called tube-representative  
 552 (TR) slip-links, which are the original slip-links finally released from the arm free end. The  
 553 other original slip-links which are destructed from the middle of the arm by CR events only  
 554 contribute to stress relaxation. For determining the terminal relaxation time of the arm  
 555 end-to-end vector, we only need to find the moment when the last tube segment held in  
 556 between the branch point and the innermost TR slip-link is released by the arm free end.

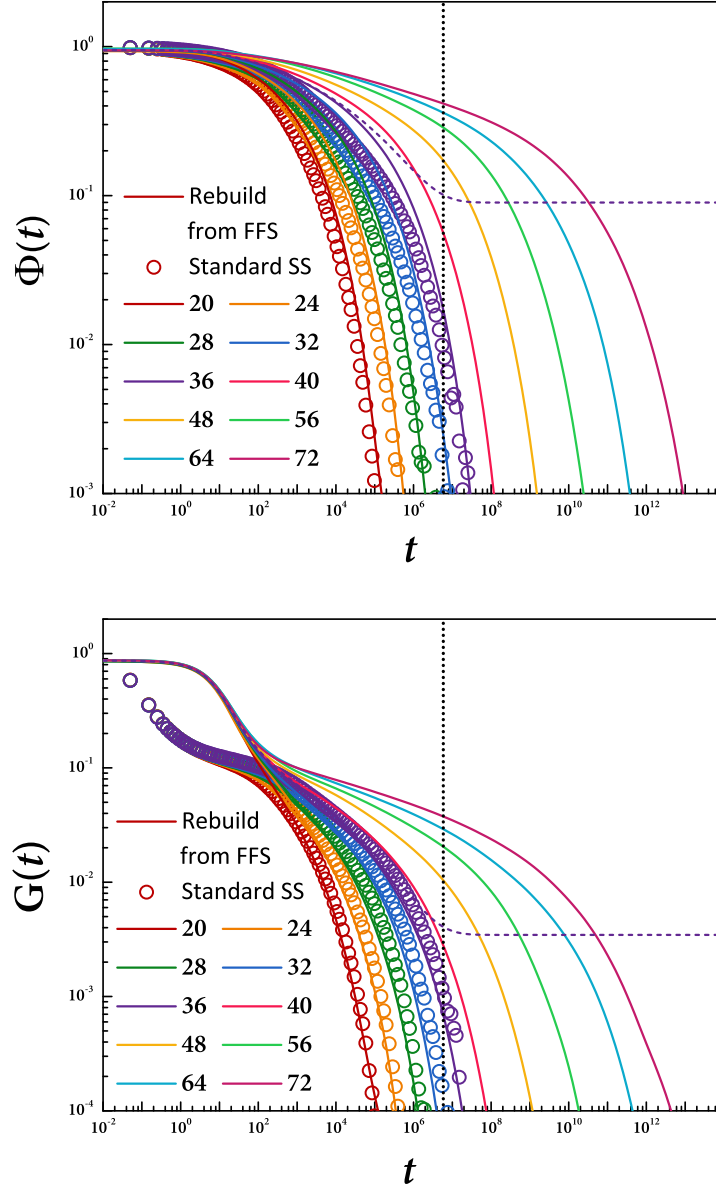


FIG. 11. (a) Arm end-to-end vector correlation function  $\Phi(t)$  and (b) stress relaxation function  $G(t)$  obtained from standard slip-spring simulations (symbols) and calculated using Eq. 15 in the revised manuscript from the rebuilt trajectories (solid lines), respectively. The dashed lines represent the results on the systems with arm length  $N = 36$  calculated by using Eq. 14 directly with the  $W_m$  term included. The vertical dotted lines mark the terminal relaxation time  $\tau_d$  of arms with  $N = 36$  as determined in the FFS simulations.

557 Since it is not known in advance whether an original slip-link will be deleted by the arm  
558 end or by CR, we can define the reaction coordinate as the index of the monomer that the  
559 innermost *surviving* original slip-link sits on. In other words, if at time  $t$  the innermost orig-  
560 inal slip-link was deleted by CR, the reaction coordinate will be immediately shifted from  
561 the monomer it sat on to the monomer occupied by the nearest original slip-link, because  
562 the latter becomes the innermost surviving original slip-link.

563 Different from the systems without CR where each star arm is treated independently, the  
564 FFS simulations of the systems with CR require the use of an ensemble of star polymers  
565 where the slip-links sitting on different arms are coupled with each other. In the current  
566 work, the simulated system consists of 20 three-arm star polymers with a total number of  
567  $N_{arm} = 60$  arms. The branch points of the stars are allowed to move in space. Only one  
568 randomly chosen arm out of the whole ensemble is used for the FFS study. The setup  
569 of the interfaces on this target arm is similar to that used in the non-CR case (Fig. 5).  
570 The first interface  $\lambda_0$  is set on the monomer that the initially innermost slip-link along this  
571 arm sits on, and the subsequent interfaces are placed on outer monomers with the intervals  
572 of  $l_1 = 2$  and  $l_2 = 1$ . The reaction coordinate is defined as the index of the monomer  
573 where the innermost surviving original slip-link sits on. Both the first-stage continuous and  
574 the second-stage shooting simulations are run as the standard slip-spring model simulations  
575 which involve all star polymers in the ensemble to allow for constraint release. It means that  
576 the configurations of all these polymers need to be stored in the database on each interface.  
577 If there is no reaction coordinate jumping due to CR, the shooting simulations are carried  
578 out in the same way as in the non-CR case from interface  $\lambda_i$  to  $\lambda_{i+1}$  for  $i = 1, \dots, m-1$ . But  
579 if during a shooting simulation started from interface  $\lambda_i$ , a CR event causes the jump of the  
580 reaction coordinate from the destructed innermost original slip-link to the nearest *surviving*  
581 original slip-link, the trajectory may immediately cross one or more interfaces. In this case  
582 we allow the simulation to continue until reaching the next interface, say  $\lambda_{i+j}$  with  $j \geq 2$ , and  
583 then save the configuration of the system in the database of interface  $\lambda_{i+1}$  (instead of  $\lambda_{i+j}$ ).  
584 When a shooting simulation from  $\lambda_{i+1}$  selects this configuration as its starting point, the  
585 trajectory will instantaneously reach the next interface  $\lambda_{i+2}$ , because the reaction coordinate  
586 has actually reached or crossed this interface. As a result of the successful shooting, the  
587 same configuration will be saved in the database of  $\lambda_{i+2}$ . Following similar shooting and  
588 saving processes, this configuration will be stored in the databases of all relevant interfaces

589 from  $\lambda_{i+1}$  to  $\lambda_{i+j}$  for further sampling. This approach ensures that the events that this  
 590 jumping trajectory has also successfully crossed the interfaces  $\lambda_{i+1}, \dots, \lambda_{i+j-1}$  are correctly  
 591 counted for calculating the transition probabilities between different interfaces. The FFS  
 592 run is terminated until the last surviving original slip-link is destructed by the arm free  
 593 end and so the terminal relaxation time  $\tau_d$  is reached. In each FFS run there are 20,000  
 594 samples recorded on each interface  $\lambda_i$  ( $i = 1, \dots, m - 1$ ), and the final results on  $\tau_d$  are  
 595 averaged over 1000 independent FFS runs. In the current method for the CR case, although  
 596 the simulations and data storage involve an ensemble of  $N_{arm}$  arms, only the relaxation  
 597 spectrum of the target arm can be collected in each FFS sample run. The computational  
 598 cost and memory storage requirement are thus still high for simulating systems with very  
 599 long arms. Further improvement in the efficiency of the algorithm is apparently needed.  
 600 Another possible direction is to use the single-chain slip-spring or slip-link models with  
 601 self-consistent treatment of constraint release.<sup>59</sup>

602 The ensemble-averaged terminal relaxation times,  $\tau_d$ , obtained in the FFS simulations  
 603 with the modified definition of the reaction coordinate are presented in Fig. 12, together  
 604 with the terminal relaxation times of the arm end-to-end vector relaxation functions as ob-  
 605 tained from standard slip-spring model simulations and the mean FP times of the innermost  
 606 surviving original slip-links as obtained from the direct shooting simulations. The three sets  
 607 of data show very good agreement within error bars, which effectively validates the proposed  
 608 FFS method. The combined FFS and SS method can thus provide quantitative predictions  
 609 on the terminal relaxation times of entangled star polymers either with or without CR over  
 610 a broad range of arm lengths that are surely needed for the development of quantitative  
 611 theories for entangled branched polymers. The construction of the relaxation correlation  
 612 functions,  $\Phi(t)$  and  $G(t)$ , in the CR cases is rather complicated and will be left for later  
 613 studies.

## 614 VI. CONCLUSIONS

615 We present an application of the forward flux sampling method in combination with the  
 616 slip-spring model on studying the arm retraction dynamics of entangled star polymers. The  
 617 single-chain slip-spring model originally developed for describing entangled linear polymers  
 618 has been extended to model symmetric star polymers. As a proof of concept, we start

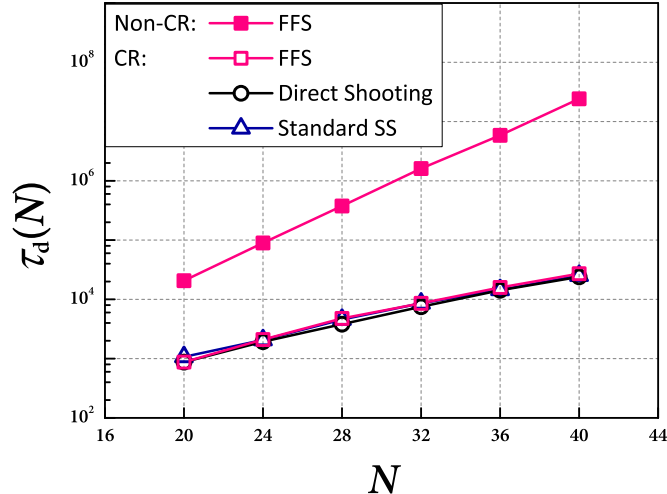


FIG. 12. Simulation results on the terminal arm relaxation times  $\tau_d$  obtained from the FFS (open squares) and direct shooting (open circles) simulations, together with the terminal times of the arm end-to-end vector correction functions calculated from standard slip-spring simulations (open triangles), in the systems with constraint release. For reference, the FFS results on  $\tau_d$  for the systems without CR (solid squares, same as in Fig. 6) are also plotted.

619 with the systems without constraint release where the entanglements or slip-links can only  
620 be created on or deleted from the arm free ends, making the FFS method conveniently  
621 applicable. Two possible reaction coordinates for the FFS simulations have been tested. The  
622 choice of the index of the monomer that the originally innermost slip-link sits on is found  
623 to provide FFS simulation results on terminal relaxation times  $\tau_d$  in good agreement with  
624 those obtained in direct shooting simulations for mildly entangled stars with arm lengths  
625 up to 8 entanglements. The FFS simulations are then performed to study the terminal  
626 relaxation of much longer arms (up to 16 entanglements) that are hardly accessible by any  
627 direct simulations, especially considering the exponential growth of  $\tau_d$  with the arm length  
628 in the absence of CR. The FFS results on  $\tau_d$  over such a broad range of arm lengths allow  
629 direct comparison with the predictions of theoretical models which are typically developed  
630 for well-entangled polymers. The entanglement molecular weight  $N_e$  extracted from such  
631 comparison is found to have an arm-length dependence.

632 In addition to the terminal arm relaxation time, the first-passage times of all other origi-  
633 nal slip-links on a given arm can also be conveniently calculated by defining the reaction  
634 coordinate as the index of the monomer that the interested slip-link sits on, which in turn

635 provides the entire relaxation spectrum of the arm. For mildly entangled arms the FFS  
636 results on the FP times show good agreement with direct shooting simulation data for the  
637 deep entanglements or inner slip-links, but some discrepancy exists for the shallow ones, be-  
638 cause the FFS method does not work well at low entropic barriers. The reliable relaxation  
639 spectrum of long star arms thus should be constructed by combining the FP times of the in-  
640 ner slip-links as calculated by the FFS method with the FP times of the outer ones obtained  
641 from direct simulations. Furthermore, we have proposed a numerical route to construct the  
642 arm relaxation correlation functions from the FFS simulation data saved on discrete inter-  
643 faces. This method is essentially a summation of weighted exponential relaxation functions  
644 with characteristic times determined by the mean FP times of different slip-links along the  
645 arm. The so-constructed arm end-to-end vector correlation functions,  $\Phi(t)$ , and stress re-  
646 laxation functions,  $G(t)$ , show reasonably good agreement with those obtained in standard  
647 slip-spring simulations in the terminal regime, while the noticeable discrepancy at short time  
648 scales can be attributed to the use of a too strong assumption that the first-passage times  
649 at the first few FFS interfaces follow the exponential distribution.

650 We have also attempted to extend the FFS method to systems with constraint release,  
651 namely to entangled star polymer melts. The key change from the non-CR case is to define  
652 the reaction coordinate using the innermost surviving original slip-link. Again good agree-  
653 ment is found between the FFS simulation results on the terminal arm relaxation time with  
654 those obtained in standard slip-spring model simulations. Therefore the combined FFS and  
655 slip-spring simulation method provides an efficient tool for studying the dynamics of highly  
656 entangled branched polymers which are generally inaccessible to direct simulation meth-  
657 ods but highly desired for the development of quantitative theories on entangled branched  
658 polymers.

## 659 **Author Information**

660 Corresponding Author: \* Email: zuowei.wang@reading.ac.uk

## 661 **ACKNOWLEDGMENTS**

662 We thank Daniel Read and Patrick Ilg for helpful discussions. This work was supported by  
663 the Engineering and Physical Sciences Research Council (EPSRC), Grant EP/K017683/1.

664 **REFERENCES**

- 665 <sup>1</sup>P. G. de Gennes, *J. Chem. Phys.* **55**, 572 (1971).
- 666 <sup>2</sup>M. Doi and S. F. Edwards, *The Theory of Polymer Dynamics* (Oxford University Press,  
667 1988).
- 668 <sup>3</sup>A. E. Likhtman and T. C. B. McLeish, *Macromolecules* **35**, 6332 (2002).
- 669 <sup>4</sup>S. Milner and T. McLeish, *Macromolecules* **30**, 2159 (1997).
- 670 <sup>5</sup>S. Milner and T. McLeish, *Phys. Rev. Lett.* **81**, 725 (1998).
- 671 <sup>6</sup>S. T. Milner and J. D. Newhall, *Phys. Rev. Lett.* **105**, 208302 (2010).
- 672 <sup>7</sup>M. Doi and N. Y. Kuzuu, *J. Polym. Sci., Polym. Lett. Ed.* **18**, 775 (1980).
- 673 <sup>8</sup>D. S. Pearson and E. Helfand, *Macromolecules* **17**, 888 (1984).
- 674 <sup>9</sup>R. Ball and T. McLeish, *Macromolecules* **22**, 1911 (1989).
- 675 <sup>10</sup>G. Marrucci, *J. Polym. Sci., Polym. Phys. Ed.* **23**, 159 (1985).
- 676 <sup>11</sup>A. L. Frischknecht, S. T. Milner, A. Pryke, R. N. Young, R. Hawkins, and T. C. B.  
677 McLeish, *Macromolecules* **35**, 4801 (2002).
- 678 <sup>12</sup>R. G. Larson, *Macromolecules* **34**, 4556 (2001).
- 679 <sup>13</sup>S. J. Park, S. Shanbhag, and R. G. Larson, *Rehol. Acta* **44**, 319 (2005).
- 680 <sup>14</sup>C. Das, N. J. Inkson, D. J. Read, M. A. Kelmanson, and T. C. B. McLeish, *J. Rheol.* **50**,  
681 207 (2006).
- 682 <sup>15</sup>E. van Ruymbeke, C. Bailly, R. Keunings, and D. Vlassopoulos, *Macromolecules* **39**, 6248  
683 (2006).
- 684 <sup>16</sup>Z. Wang, X. Chen, and R. G. Larson, *J. Rheol.* **54**, 223 (2010).
- 685 <sup>17</sup>P. S. Desai, B.-G. Kang, M. Katzarova, R. Hall, Q. Huang, S. Lee, M. Shivokhin, T. Chang,  
686 D. C. Venerus, J. Mays, J. D. Schieber, and R. G. Larson, *Macromolecules* **49**, 4964 (2016).
- 687 <sup>18</sup>J. Cao, J. Zhu, Z. Wang, and A. E. Likhtman, *J. Chem. Phys.* **143**, 204105 (2015).
- 688 <sup>19</sup>C. C. Hua and J. D. Schieber, *J. Chem. Phys.* **109**, 10018 (1998).
- 689 <sup>20</sup>Y. Masubuchi, J.-I. Takimoto, K. Koyama, G. Ianniruberto, G. Marrucci, and F. Greco,  
690 *J. Chem. Phys.* **115**, 4387 (2001).
- 691 <sup>21</sup>J. D. Schieber, J. Neergaard, and S. Gupta, *J. Rheol.* **47**, 213 (2003).
- 692 <sup>22</sup>Y. Masubuchi, G. Ianniruberto, F. Greco, and G. Marrucci, *J. Chem. Phys.* **119**, 6925  
693 (2003).
- 694 <sup>23</sup>Y. Masubuchi, G. Ianniruberto, F. Greco, and G. Marrucci, *Modell. Simul. Mater. Sci.*



695 Eng. **12**, S91 (2004).

696 <sup>24</sup>T. Yaoita, T. Isaki, Y. Masubuchi, H. Watanabe, G. Ianniruberto, F. Greco, and G. Mar-  
697 rucci, *J. Chem. Phys.* **121**, 12650 (2004).

698 <sup>25</sup>A. E. Likhtman, *Macromolecules* **38**, 6128 (2005).

699 <sup>26</sup>M. Shivokhin, E. Van Ruymbeke, C. Bailly, D. Kouloumasis, N. Hadjichristidis, and A. E.  
700 Likhtman, *Macromolecules* **47**, 2451 (2014).

701 <sup>27</sup>E. Pilyugina, M. Andreev, and J. D. Schieber, *Macromolecules* **45**, 5728 (2012).

702 <sup>28</sup>V. C. Chappa, D. C. Morse, A. Zippelius, and M. Müller, *Phys. Rev. Lett.* **109**, 148302  
703 (2012).

704 <sup>29</sup>S. K. Sukumaran and A. E. Likhtman, *Macromolecules* **42**, 4300 (2009).

705 <sup>30</sup>Z. Wang, A. E. Likhtman, and R. G. Larson, *Macromolecules* **45**, 3557 (2012).

706 <sup>31</sup>M. Wang, A. E. Likhtman, and B. D. Olsen, *ACS Macro Lett.* **4**, 242 (2015).

707 <sup>32</sup>A. E. Likhtman, in *Polymer Science: A Comprehensive Reference* (Elsevier B.V., 2012).

708 <sup>33</sup>A. V. Brukhno, J. Anwar, R. Davidchack, and R. Handel, *J. Phys. Condens. Matter* **20**,  
709 494243 (2008).

710 <sup>34</sup>D. Quigley and P. M. Rodger, *J. Chem. Phys.* **128**, 154518 (2008).

711 <sup>35</sup>R. J. Allen, P. B. Warren, and P. R. Ten Wolde, *Phys. Rev. Lett.* **94**, 018104 (2005).

712 <sup>36</sup>A. Borgia, P. M. Williams, and J. Clarke, *Annu. Rev. Biochem.* **77**, 101 (2008).

713 <sup>37</sup>T. Li, D. Donadio, G. Russo, and G. Galli, *Phys. Chem. Chem. Phys.* **13**, 19807 (2011).

714 <sup>38</sup>G. M. Torrie and J. P. Valleau, *J. Comput. Phys.* **23**, 187 (1977).

715 <sup>39</sup>C. Dellago, P. G. Bolhuis, F. S. Csajka, and D. Chandler, *J. Chem. Phys.* **108**, 1964  
716 (1998).

717 <sup>40</sup>R. J. Allen, C. Valeriani, and P. R. ten Wolde, *J. Phys. Condens. Matter* **21**, 463102  
718 (2009).

719 <sup>41</sup>K. Kratzer, A. Arnold, and R. J. Allen, *J. Chem. Phys.* **138**, 164112 (2013).

720 <sup>42</sup>E. E. Borrero and F. A. Escobedo, *J. Chem. Phys.* **125**, 164904 (2006).

721 <sup>43</sup>J. T. Berryman and T. Schilling, *J. Chem. Phys.* **133**, 244101 (2010).

722 <sup>44</sup>N. B. Becker, R. J. Allen, and P. R. ten Wolde, *J. Chem. Phys.* **136**, 05B607 (2012).

723 <sup>45</sup>B. W. Zhang, D. Jasnow, and D. M. Zuckerman, *Proc. Natl. Acad. Sci.* **104**, 18043 (2007).

724 <sup>46</sup>B. W. Zhang, D. Jasnow, and D. M. Zuckerman, *J. Chem. Phys.* **132**, 054107 (2010).

725 <sup>47</sup>G. A. Huber and S. Kim, *Biophys. J.* **70**, 97 (1996).

726 <sup>48</sup>P. E. Rouse Jr, *J. Chem. Phys.* **21**, 1272 (1953).

- 727 <sup>49</sup>A. E. Likhtman and M. Ponmurugan, *Macromolecules* **47**, 1470 (2014).
- 728 <sup>50</sup>J. Qin and S. T. Milner, *Macromolecules* **47**, 6077 (2014).
- 729 <sup>51</sup>J. Cao and Z. Wang, *Macromolecules* **49**, 5677 (2016).
- 730 <sup>52</sup>M. Shivokhin, D. Read, D. Kouloumasis, R. Kocen, F. Zhuge, C. Bailly, N. Hadjichristidis,  
731 and A. Likhtman, *Macromolecules* , In Press (2017).
- 732 <sup>53</sup>J. D. Schieber, *J. Chem. Phys.* **118**, 5162 (2003).
- 733 <sup>54</sup>M. Freidlin, J. Szucs, and A. Wentzell, *Random Perturbations of Dynamical Systems*  
734 (Springer New York, 2012).
- 735 <sup>55</sup>T. C. B. McLeish, *Advances in Phys.* **51**, 1379 (2002).
- 736 <sup>56</sup>R. N. Khaliullin and J. D. Schieber, *Phys. Rev. Lett.* **100**, 188302 (2008).
- 737 <sup>57</sup>J. Ramirez, S. K. Sukumaran, and A. E. Likhtman, *J. Chem. Phys.* **126**, 244904 (2007).
- 738 <sup>58</sup>T. Uneyama and Y. Masubuchi, *J. Chem. Phys.* **137**, 154902 (2012).
- 739 <sup>59</sup>R. N. Khaliullin and J. D. Schieber, *Macromolecules* **42**, 7504 (2009).